Provided for non-commercial research and education use. Not for reproduction, distribution or commercial use.



This article appeared in a journal published by Elsevier. The attached copy is furnished to the author for internal non-commercial research and education use, including for instruction at the authors institution and sharing with colleagues.

Other uses, including reproduction and distribution, or selling or licensing copies, or posting to personal, institutional or third party websites are prohibited.

In most cases authors are permitted to post their version of the article (e.g. in Word or Tex form) to their personal website or institutional repository. Authors requiring further information regarding Elsevier's archiving and manuscript policies are encouraged to visit:

http://www.elsevier.com/authorsrights

ORIGINALARBEIT

Conversion factors for determining organ doses received by paediatric patients in high-resolution single slice computed tomography with narrow collimation $^{\,\!\!\!\!/}$

Michael C. Seidenbusch 1,*, Dietrich Harder 2, Dieter F. Regulla 3, Karl Schneider 1

Received 22 March 2013; accepted 6 February 2014

Abstract

Estimations of organ doses D_T received during computed tomographic examinations are usually performed by applying conversion factors to basic dose indicators like the computed tomography dose index (CTDI) or the dose-length-product (DLP). In addition to the existing conversion factors for beam apertures of 5 mm or 10 mm, we present new DLP-D_T conversion factors adapted to high-resolution CT (HRCT) examinations of infants and young children with beam apertures of the order of 1 mm and under consideration of bow tie filtration. Calculations are performed on mathematical MIRD phantoms for an age range from 0, 1, 5, 10, 15 up to (for comparison) 30 years by adapting PCXMC, a Monte Carlo algorithm originally developed by STUK (Helsinki, Finland) for dose reconstructions in projection radiography. For this purpose, each single slice CT examination is approximated by a series of corresponding virtual planar radiographies comprising all focus positions. The transformation of CT exposure parameters into exposure parameters of the series of corresponding planar radiographies is performed by a specially developed algorithm called XCT. The DLP values are evaluated using the EGSRay code. The new method is verified Konversionsfaktoren zur Ermittlung von Organdosen bei pädiatrischen Patienten in der hochauflösenden Einzelschicht-Computertomographie mit enger Kollimation

Zusammenfassung

Die Abschätzung der vom Patienten im Rahmen computertomographischer Untersuchungen in einzelnen Organen aufgenommenen Strahlendosen (D_T) erfolgt üblicherweise durch die Anwendung von Konversionsfaktoren, wobei der Computertomographie-Dosis-Index (CTDI) oder das Dosis-Längen-Produkt (DLP) als Ausgangsdosisgrößen dienen. In dieser Arbeit werden zusätzlich zu den bereits für Schichtkollimationen von 5 mm und 10 mm existierenden Konversionsfaktoren neue DLP-D_T-Konversionsfaktoren unter Zugrundelegung einer Schichtkollimation von 1 mm und unter Berücksichtigung der Fächerstrahlfilterung für hochauflösende CT-Untersuchungen (HRCT) von Säuglingen und Kleinkindern bestimmt. Die Berechnung der Organdosen D_T wurde an mathematischen MIRD-Phantomen der Altersstufen 0, 1, 5, 10, 15 und (zum Vergleich) 30 Jahre durch Adaptation des von

¹ Paediatric Radiology, Institute for Clinical Radiology, Dr. von Hauner's Children's Hospital, Ludwig-Maximilians-University Munich, Lindwurmstr. 4, 80337 Munich, Germany

² Medical Physics and Biophysics, Georg-August-University Göttingen, Konrad-Adenauer-Str. 26, 37075 Göttingen, Germany

³ Research Unit Medical Radiation Physics and Diagnostics, Helmholtz Zentrum München - German Research Center for Environmental Health, Ingolstädter Landstr. 1, 85764 Neuherberg, Germany

[☆] ISIMEP-Projekt des Bundesministeriums für Bildung und Forschung, Förderkennzeichen 02NUK016A.

^{*}Corresponding author: Michael C. Seidenbusch, Paediatric Radiology, Institute for Clinical Radiology, Dr. von Hauner's Children's Hospital, Ludwig-Maximilians-University, Munich, 80337 Munich, Germany.

E-mail addresses: michael.seidenbusch@med.uni-muenchen.de (M.C. Seidenbusch), regulla@helmholtz-muenchen.de (D.F. Regulla).

at a beam aperture of 10 mm by comparison with formerly published conversion factors. We show that the higher spatial resolution leads to an enhanced DLP-D_T conversion factor if a small organ (e. g. thyroid gland, mammae, uterus, ovaries, testes) is exactly met by the chosen CT slice, while the conversion factor is drastically reduced if the chosen CT slice is positioned above or below the organ. This effect is utilized for dose-saving examinations with only a few single slices instead a full scan, which technique is applied in about 10% of all paediatric chest CT examinations.

Keywords: High-resolution CT, organ doses, dose length product, CTDI, computed tomographic dose index, conversion factors, fan beam filter

Schlüsselwörter: HRCT, Organdosen, Dosis-Längen-Produkt, CTDI, Konversionsfaktoren, Fächerstrahlfilter

der finnischen Strahlenschutzbehörde STUK (Helsinki, Finnland) ursprünglich für Dosisrekonstruktionen in

der konventionellen Projektionsradiographie entwickelten

Monte-Carlo-Algorithmus PCXMC an die in der Com-

putertomographie herrschenden Expositionsbedingungen

durchgeführt. Jede CT-Einzelschichtuntersuchung wurde

dabei durch eine Serie entsprechender, sämtliche Fokus-

positionen erfassender planarer Radiographien approximiert. Zur Transformation der CT-Expositionsparameter

in die Expositionsparameter einer entsprechenden Serie planarer Radiographien wurde der XCT-Algorithmus entwickelt. Die DLP-Werte wurden mit dem EGSRay-Algorithmus ermittelt. Zur Verifikation der neuen Methodik dient ein Vergleich der für eine Schichtkollimation von 10 mm ermittelten Konversionsfaktoren mit Literaturwerten. Es wird gezeigt, dass die höhere Ortsauflösung bei einem kleinen Organ (z. B. Schilddrüse, Brustdrüsen, Uterus, Ovarien, Testes) zu einem erhöhten DLP-D_T-Konversionsfaktor führt, falls die gewählte CT-Schicht genau dieses Organ erfasst, dass der Konversionsfaktor jedoch drastisch erniedrigt ist, wenn die gewählte CT-Schicht oberhalb oder unterhalb des Organs angeordnet wird. Dieser Effekt wirkt sich vor allem bei der dosissparenden Untersuchungstechnik der bei etwa 10% aller pädiatrischen CT-Thorax-Untersuchungen angewandten hochauflösenden Einzelschicht-CT aus, bei welcher nur wenige dünne Einzelschichten mit vergleichsweise hohem

1 Introduction

Computed tomography (CT) is a radiological procedure ranking in the upper sector of the required doses to the examined regions of the body [1]. With increasing availability of age-specific low-dose protocols, CT has come to be used more frequently in paediatric radiology [2]. On the other hand, the radiation sensitivity of children must be estimated considerably higher than that of adults [3–10]. Recently, direct epidemiologic proof has been given of a heightened risk for neoplastic diseases after CT examinations in the age range under 22 years [11,12]. Against that background, the possibility of the retrospective reconstruction of organ doses administered in a long-years practice of paediatric CT examinations - the aim of the present paper - is of significant importance for radiation safety and radiation epidemiology. The organ dose D_T is defined as the absorbed dose in an organ or tissue T, averaged over the mass of that organ or tissue. This definition is equivalent to the quotient of the energy imparted to the matter of the organ or tissue and its mass.

In paediatric radiology, CT beam apertures of about 1 mm, as implemented, e.g., in the CT scanner Philips Aura, have been used for a long time since this narrow collimation is necessarily adapted to the small sizes of anatomical structures in neonates and infants. In the literature of paediatric radiology [13], this narrow collimation approach, combined with the application of high-resolution reconstruction filters, is usually referred to as "high-resolution computed tomography" (HRCT). Moreover in some paediatric radiology departments, about 10% of all chest CT examinations are performed with a small set of narrow single slices with beam apertures of about 1 mm and - as a low-dose procedure with relatively large gaps between the single slices instead of continuous CT series [14–16]. Another feature of the narrow collimation single slice HRCT is the general choice of a relatively high tube voltage such as 120 kV [14], whereas low tube voltages such as 80 kV are normally applied in paediatric radiology. Relatively high tube voltages are used as an auxiliary means to obtain the high radiation output required to produce sufficiently low-noise detector signals in

the presence of the divergence and scattering of the narrow beams. The reconstruction of the organ doses received in paediatric CT deserves special attention because the longitudinal organ dose profile in the body as a function of slice position will reflect the narrow collimation and the intermittent gaps. It is an interesting question, whether these features offer the possibility of organ dose reduction compared with wider collimation scanners and with continuous CT series.

In most previous publications conversion factors were established for calculating the organ doses D_T from basic dose indicators capable of being measured in clinical routine like the computed tomography dose index CTDI_{air}, the CTDI_{vol} or the dose-length-product DLP [17], referring to beam apertures of more than 5 mm as well as by largely neglecting fan beam filtering. A comprehensive system of tables with values of the conversion factor k_{CTDIair,DT,j}, leading from the CTDI_{air}, for one tube rotation at slice position j to the associated organ dose contribution $D_{T,j}$, has been created in 1991 by Zankl et al. [18,19] from the Helmholtz Zentrum München (formerly the GSF National Research Center for Environment and Health, Neuherberg) and by Jones and Shrimpton [20,21] at the National Radiological Protection Board in Chilton, UK, on the basis of Monte Carlo simulations of many single slices j in mathematical phantoms and voxel phantoms. The calculations by Zankl et al. were made using a beam aperture of 10 mm as a base and by neglecting fan beam filters, while Jones and Shrimpton used a beam aperture of 5 mm and accounted for selected fan beam filters from various manufacturers. Since Monte Carlo simulations of CT examinations require high computing times, most of the clinically usable computer programmes for the reconstruction of the organ and effective doses administered in connection with clinical CT examinations are based on the tables of Zankl et al. [18,19] and Jones et al. [20,21]. Noteworthy amongst computer programmes created on that basis and commercially available are WinDose [22], CTDOSE [23], CT-Dose [24], IMPACT [25] and CT-Expo [26]. In most of these programmes, CTDI_{air,j} or DLP_i (the dose-length-product of the single slice j) are used as the basic dose indicators for the reconstruction of patient doses [27].

In consideration of the given geometric conditions, conversion factors serving in the present study to adequately reconstruct the organ doses in paediatric CT examinations are based on a beam aperture of 1 mm as the standard. These conversion factors were obtained by applying the commercially available PCXMC algorithm of the Finnish Radiation and Nuclear Safety Authority (Säteilyturvakeskus STUK, Helsinki) on the basis of Monte Carlo simulations in mathematical paediatric MIRD phantoms for age levels of 0, 1, 5, 10, 15 and (for purposes of comparison) 30 years, and by factoring in a beam aperture of 1 mm. In addition, special consideration has been given to the effect of fan beam filtering on the dose distribution in the child's body. While, in the 1990s, numerous CT scanners lacked any possibility of fan beam filtering (synonym: bow tie filtering), fan beam filters are implemented

in all modern CT equipment for technical image processing reasons. For that reason, the impact of fan beam filtering shall be illustrated in this paper with reference to the CT scanner Philips Aura.

Although the operating consoles of the currently used CT scanners generally indicate the $CTDI_{air}$ or the $CTDI_{vol}$ for one tube rotation [17], we will in this paper study the conversion factor $k_{DLP,DT,j}$ which converts the DLP_j in air, measured for slice j on the rotation axis, into $D_{T,j}$, the contribution of slice j to the dose D_T to the organ or tissue T. The DLP in air is generally defined as the line integral of the air kerma over a line parallel to the rotation axis, and the integration length has to be stated [17]. In this paper, we are in principle using an infinite integration length, e.g. in eq. (1) below, and in the numerical calculations a practical integration length of 100 mm for any DLP_j was chosen as a very good approximation to this definition.

For the narrow collimations used in paediatric HRCT, the DLP_i is frequently referred to, and it is available for retrospective studies. It is proportional to the energy input into the patient' body associated with slice j, and it can be regarded as proportional to the sum of the detector signals received and therefore as a measure of the information collected in one tube rotation. Moreover, conversion factors of the type k_{DLP,DT} are useful in numerical comparisons between conversion factors applicable to different beam apertures, in particular in our comparison with the conversion factors according to Zankl et al. [18,19] which are valid for 10 mm beam aperture. For n adjacent slices with the same DLP_i, the combined k_{DLP.DT} value for a specific organ T is the arithmetic mean of the n individual values. This can be shown for a set of n slices (j = 1...n) adjacent to each other, where $D_{T,j}$ is the organ dose contribution of slice j, and DLP_j is the DLP of the j-th slice. If all DLP_i are equal, we have

$$k_{DLP,DT} = \frac{D_T}{DLP} = \frac{\sum_{j} D_{T,j}}{n \cdot DLP_j} = \frac{\overline{D_{T,j}}}{DLP_j} = \overline{k_{DLP,DT,j}}$$
(1)

This relationship has been used in Fig. 5 for the $k_{DLP,DT}$ comparison between 10 adjacent slices of 1 mm thickness with one slice of 10 mm thickness.

As examples to illustrate the methodology used, conversion factors for several organs and varied exposure conditions will be presented for the single-slice Philips Aura CT scanner with 1 mm beam aperture operated in the Department of Paediatric Radiology at Dr. von Hauner's Children's Hospital, Munich. This paper will conclude with a view on the possibilities of dose reconstruction for other methods of paediatric CT examinations.

2 Materials and methods

2.1 Radiation field geometry

In order to derive the organ doses achieved during CT examinations, Monte Carlo simulations are generally applied [28] to realistic virtual mathematical phantoms [29,30] or to anthropomorphic voxel phantoms identical to reality [31,32]. The Monte Carlo method is based on the simulation of stochastically distributed interactions of radiation particles with matter of known chemical composition. In x-ray diagnostics it follows the histories of individual photons, starting from the appearance of a photon at the phantom surface, throughout the scattering and absorption processes and up to the deposition of energy in the phantom or detector material [33,34].

In the present study, the PCXMC algorithm from STUK, Helsinki, originally designed for the Monte Carlo simulation of dose distributions in conventional planar radiography, is applied to paediatric HRCT examinations. With the aid of the XCT algorithm developed for this purpose, the STUK-MIRD phantoms of body height H corresponding to the various age levels are mathematically divided up into 1 mm thin slices with axial slice positions $z_j~(0 \le z_j \le H).$ To each of these slices a single slice CT examination with 360° full rotation of the x-ray tube is allocated, where each single slice CT examination is composed of 360 individual fan beam exposures under the rotation angles $\omega_i~(1^\circ \le \omega_i \le 360^\circ).$ In that way, each single slice CT examination is replaced with a set of 360 planar radiographies under the projection angles $\omega_i~(1^\circ \le \omega_i \le 360^\circ).$

The spatial visualization of the position of a single fan beam in relation to the MIRD phantom in Fig. 1 shows the source-to-skin distance $SSD(\omega_i)$, the body diameter $d(\omega_i)$ along the central beam, the field width $w(\omega_i)$ in the plane of incidence and the field height $h(\omega_i)$ in the plane of incidence in the direction of the rotation axis, all of them in functional dependence upon the projection angle (i.e. the rotation angle of the x-ray tube) ω_i . Also shown are the intersection length s of the fan

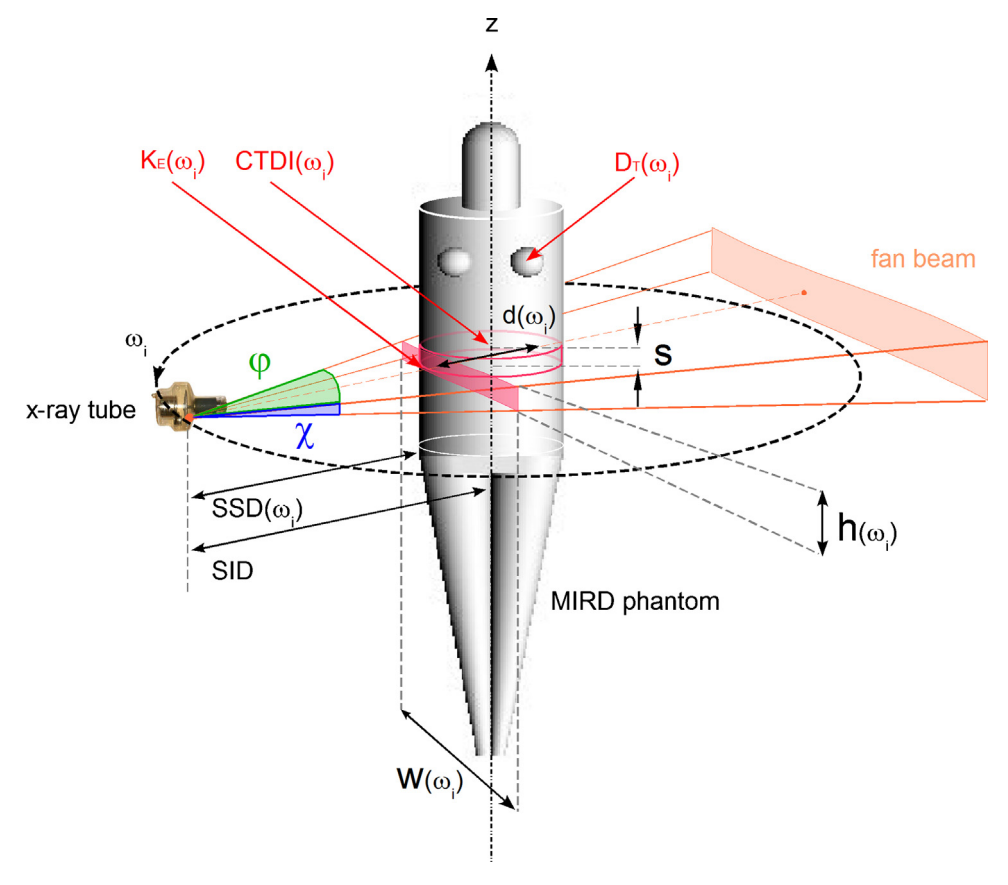


Figure 1. Beam geometry of a single slice CT examination and of the corresponding planar projection radiography. The characteristic quantities of the CT exposure geometry are the gantry rotation angle ω_i , the transversal width angle of the fan beam (fan beam angle) φ , the axial width angle of the fan beam (fan beam aperture) χ , the slice collimation s, and the focus-isocentre distance SID. The characteristic quantities of the equivalent planar radiography exposure are the projection angle ω_i , the field width w_i , the field height h_i , and the source-skin distance SSD_i. The relationship between the two exposure geometries is given by the rotation angle dependent patient diameter $d(\omega_i)$. The dosimetric characteristics are the incidence dose $K_E(\omega_i)$, the CTDI(ω_i), and the associated partial organ dose $D_T(\omega_i)$, here indicated for T = mammae as an example.

beam (identical for all 360 fan beams) along the rotation axis (equivalent to the axial width angle of the fan beam χ the so-called "beam aperture"), the transversal width angle ϕ of the fan beam (the so-called "fan beam angle") and the source-to-isocentre distance SID. Further indicated are the values $CTDI(\omega_i)$ to be calculated and an example for an organ dose $D_T(\omega_i)$ as well as the incidence dose $K_E(\omega_i)$ at the phantom surface, serving in this study as an auxiliary variable.

For each single fan beam exposure i it is necessary to calculate the parameters of the conventional planar radiography equivalent to it, namely $SSD(\omega_i)$, $h(\omega_i)$ and $w(\omega_i)$ from the geometric parameters of the fan beam, SID, s, ω_i and ϕ :

$$SSD(\omega_i) = SID - \frac{d(\omega_i)}{2} \tag{2}$$

$$h(\omega_i) = s \cdot \left(1 - \frac{d(\omega_i)}{2 \cdot SID}\right) \tag{3}$$

$$w(\omega_i) = 2 \cdot (SID - d(\omega_i)) \cdot \tan\left(\frac{\varphi}{2}\right) \tag{4}$$

2.2 Schedule for the calculation of conversion factors

The dose length product DLP_j and the organ dose $D_{T,j}$ associated with a slice j result from summations over the contributions from all rotation angles ω_i :

$$DLP_{j} = \sum_{i=1}^{360} DLP_{i,j}$$
 (5)

$$D_{T,j} = \sum_{i=1}^{360} D_{T,i,j} \tag{6}$$

with the conversion factor $k_{DLP,DT,j}$ defined through the relationship

$$D_{T,j} = k_{DLP,DT,j} \cdot DLP_j \tag{7}$$

In our calculation, where two different algorithms are combined to calculate DLP_j and $D_{T,j}$, the incidence dose $K_{E,j}$ serves to link the two component calculations as follows: For each fan beam i, j (rotation angle ω_i , slice z_j) the relation is established between its contribution to the dose-length-product, $DLP_{i,j}$, and its contribution to the incidence dose, $K_{E,i,j}$:

$$DLP_{i,j} = k_{KE,DLP,i,j} \cdot K_{E,i,j} \tag{8}$$

This is achieved by calculation with the EGSRay algorithm as described in section 2.3. The conversion factors $k_{\text{KE,DLP},i,j}$ were calculated from the kerma distributions in air given by the EGSRay Monte Carlo simulations.

On the other hand, for each fan beam i, j the relationship between the contribution to the organ dose, $D_{T,i,j}$, and the contribution to the incidence dose, $K_{E,i,j}$, is established:

$$D_{T,i,j} = k_{KE,DT,i,j} \cdot K_{E,i,j} \tag{9}$$

This is achieved by calculation with the PCXMC algorithm described in section 2.4. Combining eq. (5) and (8) we can then derive:

$$k_{KE,DLP,j} = \frac{\sum_{i=1}^{360} k_{KE,DLP,i,j} \cdot K_{E,i,j}}{\sum_{i=1}^{360} K_{E,i,j}}$$
(10)

and from eq. (6) and (9) we have

$$k_{KE,DT,j} = \frac{\sum_{i=1}^{360} k_{KE,DT,i,j} \cdot K_{E,i,j}}{\sum_{i=1}^{360} K_{E,i,j}}$$
(11)

Finally with eq. (7), (10) and (11) we get the sought conversion factor for a single slice j:

$$k_{DLP,DT,j} = \frac{k_{KE,DT,j}}{k_{KE,DLP,j}} \tag{12}$$

For a series of slices j, all with the same DLPj, we can use eq. (1) in addition to eq. (12). The calculation of the conversion factors according to equations (10) to (12) was accomplished with the XCT algorithm. The conversion factors for individual slices, $k_{DLP,DT,j}$ (eq. 12) will be illustrated by a series of examples in the results section 3.2 (Fig. 5.a-d).

2.3 Conversion factors for converting the incidence dose into the dose-length product (EGSRay algorithm)

The freely available EGSRay algorithm is based on the EGS4 code [35] and was adapted by *Kleinschmidt* [36] for clinical applications. The algorithm allows, inter alia, for Monte Carlo simulations of spatial air kerma distributions for random radiation sources, qualities and geometries. To determine the conversion factors according to eq. (6), in accordance with the parameters derived by equations (2) through (4), a fan beam was defined and, for that fan beam, Monte Carlo simulations with the aid of the EGS-Ray algorithm were used to

determine spatial distributions of the air kerma for 10⁹ photons. The air kerma readings were obtained for focus-to-skin distances resulting from different tube rotation angles, and the DLP on the rotation axis was obtained by integrating the profile of the air kerma along the rotation axis over a length of 100 mm [17].

2.4 Conversion factors for converting the incidence dose into the organ dose (PCXMC algorithm)

With the commercially available PC software PCXMC developed by STUK, Helsinki, an efficient algorithm was created to conduct Monte Carlo simulations in conventional radiology [37,38]. Implemented in the algorithm is a complete phantom family of mathematical hermaphrodite MIRD phantoms at age levels of 0, 1, 5, 10, 15 and 30 years in accordance with the models given by Cristy et al. [39] and the ICRP standard [40] (Figs. 2 and 3). The algorithm has already been successfully used to determine new conversion factors for conventional paediatric radiography [41–44]. The software version 1.5.1 was used for calculation of the conversion factors according to eq. (7), since in the expanded 2.0 version of this programme [45] in the MIRD phantoms the rotation symmetry of the cranium suitable for calculating the cranium

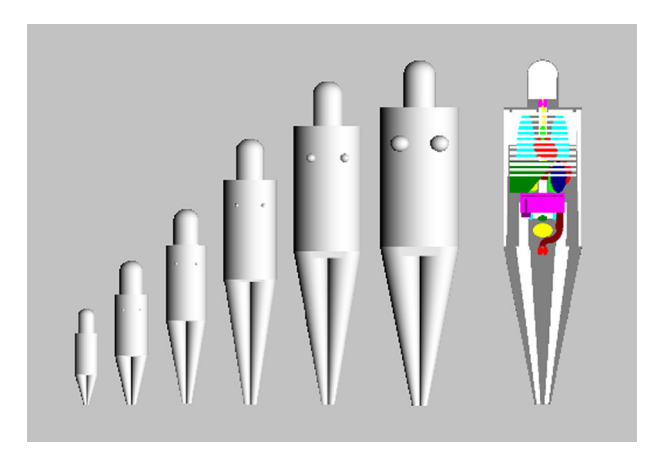


Figure 2. STUK-MIRD phantom family, consisting of phantoms of ages 0, 1, 5, 10, 15 and 30 years. The organ situs is shown in the adult phantom (right).

dose in CT has been replaced by (more realistic) asymmetric design.

All Monte Carlo simulations were based on the planar beam geometries according to equations (2) through (5) taking the geometry of the equipment of the Philips single-slice

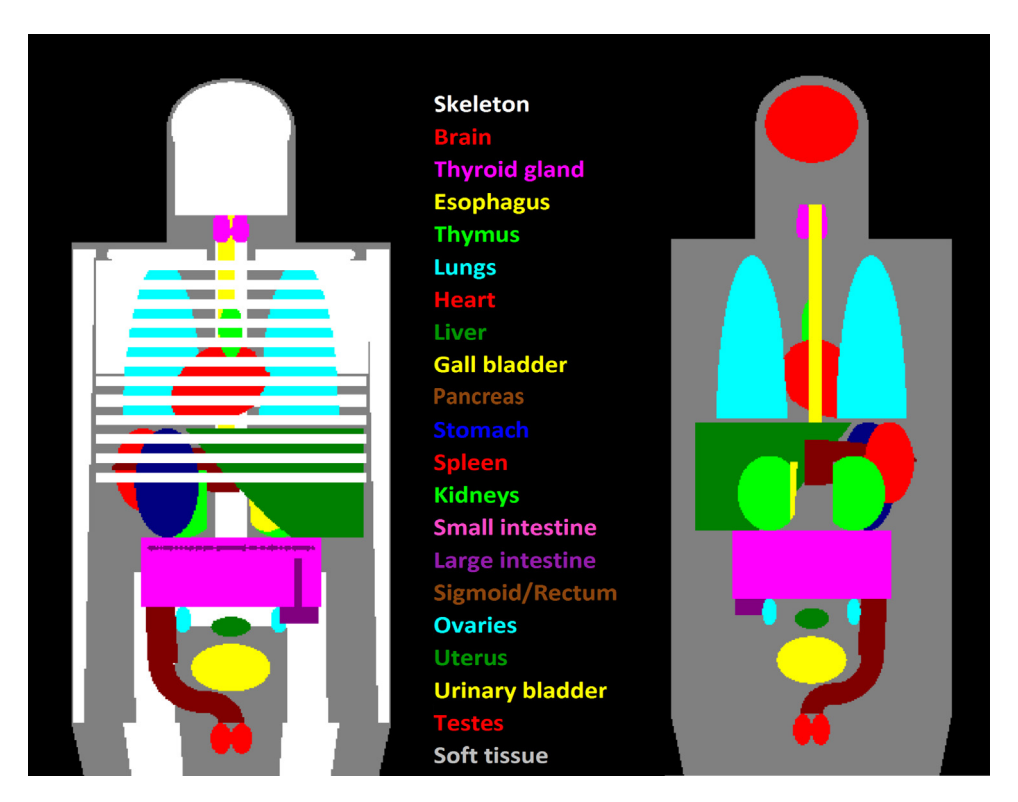


Figure 3. The organs and tissues of the hermaphroditic mathematical STUK-MIRD phantoms (white=skeleton; grey=soft tissues; red=brain, heart, spleen, scrotum; yellow=esophagus, gall bladder, urinary bladder; light green=thymus, kidneys; dark green=liver, uterus; light blue=lungs, ovaries; dark blue=stomach; brown=pancreas, colon sigmoideum, rectum; pink=thyroidea, intestinum; purple=colon). For better visualization of organ positions, skelettal structures were left out in the pa projection (right). Reference organs not displayed in these projections, but considered in the calculations are mammae, skin, muscular tissue and red bone marrow.

Table 1 Exposure parameters of the CT scanner Philips Aura and exposure parameters of the scanner geometry considered by Zankl et al. [18,19] as they were used for the Monte Carlo simulations.

| | CT Philips Aura | Zankl et al. |
|-----------------------------------|-----------------------------|-------------------|
| Focus-isocentre distance SID | 51.5 cm | 70 cm |
| Fan beam angle φ | 47.2°/ 52° (mean value 50°) | 40° |
| Beam aperture (slice thickness) s | 1 mm | - |
| | 10 mm | 10 mm |
| Tube voltage | 120 kV | 125 kV |
| Total filtration | 1.5 Al + 0.07 mm | 2.2 Al + 0.2 mm |
| | Cu | Cu |
| Fan beam filtering | yes | no |
| Normalized CTDI in air | 0.41 mGy/mAs | - |

Aura CT scanner from Philips Company, Netherlands, year of construction 2002, into account (Table 1). For each virtual planar radiography, Monte Carlo simulations of radiation energy deposition in all of the approximately 40 organs and tissues of the mathematical MIRD phantoms of all age levels were carried out, based on beam apertures of 1 mm and 10 mm, even if the organs and tissues were not directly covered by the primary radiation field. For each HRCT single slice a total of $360 \cdot 10^4$ individual photon histories was considered.

2.5 Consideration of the fan beam filtering

The procedure to determine CT conversion factors according to equations (6) and (7) also allows to consider fan beam filtering. Fan beam filtering has the effect, inside a given fan beam, of an angle-dependent modification of the spatial distribution of air kerma. In the Monte Carlo simulations such angle-dependent air kerma distributions can be factored in by

means of a subdivision of the entire fan beam into several disjointed partial fan beam bundles. For reasons of symmetry, subdivision has been undertaken in this study of fan beam i with fan beam angle φ into a total of 9 disjointed partial fan beam bundles k=1...9 with corresponding fan beam angles of $\varphi/9$. In that way, the factors to be used in eq. (10) and (11) are obtained by:

$$k_{KE,DLP,i,j} = \frac{\sum_{k} k_{KE,DLP,i,j,k} \cdot K_{E,i,j,k}}{\sum_{k} K_{E,i,j,k}}$$
(13)

and

$$k_{KE,DT,i,j} = \frac{\sum_{k} k_{KE,DT,i,j,k} \cdot K_{E,i,j,k}}{\sum_{k} K_{E,i,j,k}}$$
(14)

Specific conversion factors
$$\sum_{i,j,k} k_{KE,DT,i,j,k}$$
 and

 $\sum_{i,j,k} k_{KE,DLP,i,j,k}$ for specific fan beam filtrations can be

determined by Monte Carlo simulations for the partial fan beam bundles, taking the underlying form filter data into account. In this study, for exemplification purposes, new conversion factors have been determined for the Philips Aura CT scanner used here as a reference model.

3 Results

3.1 Dose profiles in air

Several examples of the calculation with the EGSRay algorithm described in section 2.3 are shown in Fig. 4 using the

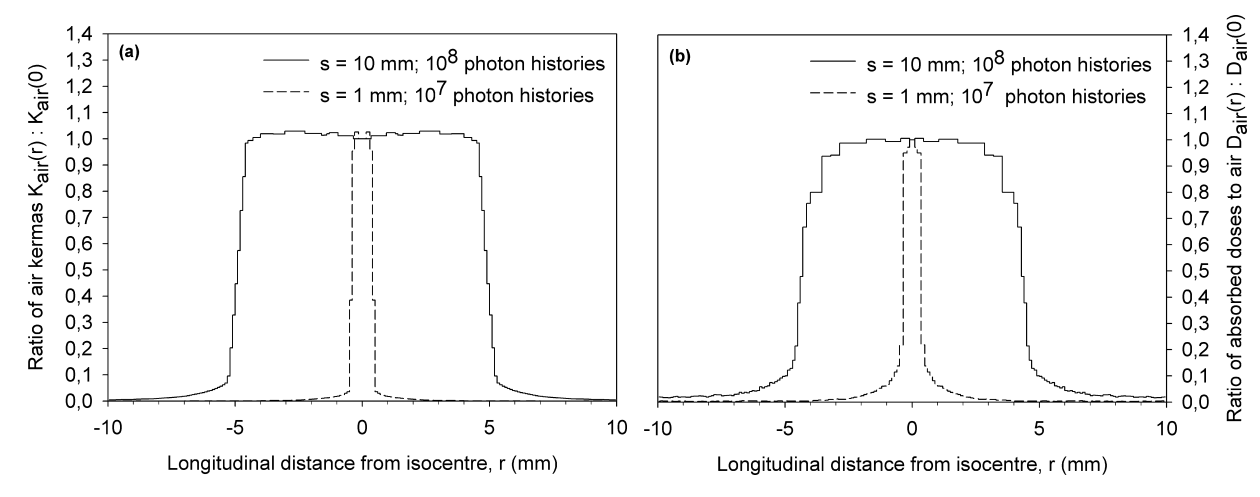


Figure 4. Air kerma profiles (a) and absorbed dose to air profiles (b) in the direction of the rotation axis. They are valid for the radiation incidence plane of a water phantom (d = 20.4 cm) centered in the isocentre, corresponding to a 10 year old patient, at SID = 70 cm and SSD = 60 cm. The slice collimation was either s = 1 mm or s = 10 mm. The radiation quality was 125 kV + 2.2 mm Al + 0.2 mm Cu.

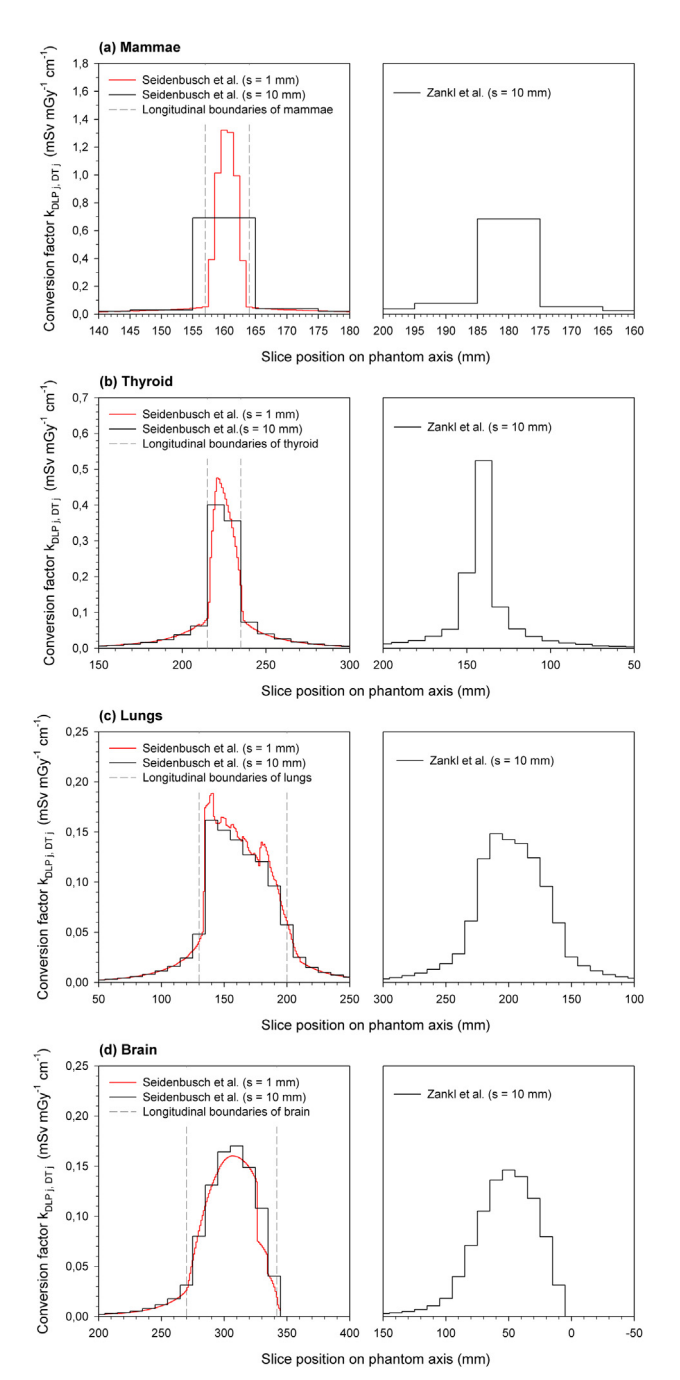


Figure 5. Conversion factors $k_{\mathrm{DLP_{j},DT_{j}}}$ of a neonate plotted as function of the position of slice j on the phantom axis for slice collimations $s = 1 \,\mathrm{mm}$ (red) and $s = 10 \,\mathrm{mm}$ (black) at radiation quality 125 kV + 2.2 mm Al + 0.2 mm Cu. Computed results of this paper (left) are compared with the results of Zankl et al. [18,19] (right). The longitudinal extension of each organ is indicated by the grey dashed lines. Note that the longitudinal axis of the STUK-MIRD phantoms goes from caudal to cranial with the origin located at the middle of the base of the trunk and that of the anthropomorphic voxel phantoms used by Zankl et al. goes from cranial to caudal with the origin located at the top of the skull. If the DLP_j values of all 1 mm slices

Table 2
Maximal longitudinal diameters of selected organs of the STUK-MIRD phantoms.

| Age (years) | Maximal longitudinal diameter (mm) | | | |
|-------------|------------------------------------|---------|-------|-------|
| | Mamma | Thyroid | Lungs | Brain |
| 0 | 7 | 20 | 70 | 72 |
| 1 | 12 | 22 | 105 | 98 |
| 5 | 16 | 28 | 140 | 110 |
| 10 | 18 | 36 | 174 | 113 |
| 15 | 41 | 42 | 205 | 115 |
| 30 | 81 | 50 | 240 | 115 |

examples of air kerma and absorbed dose to air in the entry plane of the phantom. The air kerma profiles show weak lateral tails due to the "geometric penumbra", resulting from the focus size, and to photon scattering at the collimator edges. The profiles of the absorbed dose to air are furthermore smoothened by secondary electron transport in air. From graphs of this type the contribution of each fan beam bundle to the air kerma in the entry plane and to the dose-length-product on the rotation axis can be read out. This yields the air kerma values used in equations (6) and (7).

3.2 Impact of beam aperture and slice position on the dose profiles in selected neonate organs

In the following, conversion factors calculated under the exposure conditions considered by Zankl et al. [13,14], listed in the right column of Table 1, for CT examinations with single slices of 1 mm and 10 mm thickness in child patients will be studied in detail, taking as examples in the order of increasing axial thickness the mammae, the thyroid, the lungs and the brain. The study will particularly refer to a neonate or a young infant for whom narrow collimation single slice HRCT examinations are indicated, for instance, due to interstitial lung diseases. For the organs in question, the maximum organ diameters on the longitudinal axis of the STUK-MIRD phantoms, depending upon age level, are listed in Table 2.

In Fig. 5 the values of the conversion factor $k_{DLP,DT,j}$, i.e. the quotient of the partial organ dose $D_{T,j}$ produced by the single slice j and the dose-length-product DLP_j belonging to the same slice and computed by eq. (12), are shown. The partial organ dose $D_{T,j}$ is the contribution to the entire organ dose D_T associated with slice j within a series of slices. With all organs, arranged in a sequence according to the maximum longitudinal diameter of the organ (7 mm in the mammae, 20 mm in the thyroid, 70 mm in the lungs and 72 mm in the brain), and with a slice thickness of 1 mm, the topological gradation of the partial organ doses $D_{T,j}$ can be identified depending on the position of slice j. For the lung organ dose, the shielding of the

were assumed to be equal, Fig. 5 would also show the longitudinal profiles of the contributions $D_{T,j}$ to the organ doses D_T .

lungs by the ribs comes out in the form of somewhat reduced D_{Ti} readings when the fan beam is localised over the ribs, while the brain shows an abrupt break-off of the dose values when the slice is positioned at the cranial end of the body. As an organ or tissue is not only met by the primary field of radiation but also by scattered radiation, the dose profile does not immediately fall to zero when the slice j is localized outside the longitudinal boundaries of the organ or tissue. If the slice thickness is increased from 1 mm to 10 mm and the addition of the D_{T,i} values and the DLP_i values of the ten 1 mm slices is expressed by eq. (1), then the gradation in the D_{Ti} values becomes correspondingly rougher. For 10 adjacent 1 mm slices with the same DLP_i, combined to form a 10 mm slice, there is good agreement of the mean values of the conversion coefficient computed according to eq. (1) with the 10 mm values given by Zankl et al. [18,19]. Minor differences are explained by somewhat different organ dimensions in the anthropomorphic voxel phantoms used by Zankl et al. Furthermore, the longitudinal axis of the STUK-MIRD phantoms used in this study goes from caudal to cranial with the origin located at the middle of the base of the trunk and that of the anthropomorphic voxel phantoms used by Zankl et al. [18,19] goes from cranial to caudal with the origin located at the top of the skull.

The conversion factors calculated on the basis of a beam aperture of 1 mm correspond to the higher spatial resolution: For small organs, particularly noticeable in case of the mammae, the conversion factor from DLP to the partial organ dose for a 1 mm slice directly placed upon the organ is *higher* by a factor of approximately 2 compared with the 10 mm slice, since only part of the latter is overlapping with the organ. If, on the other hand, the 1 mm slice is placed directly above

or below to the small organ, then the concomitant conversion factor from DLP to the partial organ dose is considerably *lower* than that produced by the 10 mm wide slice as long as it continues to overlap with the small organ.

3.3 Impact of fan beam filtering on the dose profiles in infants

The organ dose profiles shown in section 3.2 were calculated for fan beams without fan beam filtering. To take the latter into account, the conversion factors according to equations (13) and (14) were derived on the basis of air kerma profiles as they emerge from Monte Carlo simulations with the aid of the EGSRay algorithm when the exposure conditions and the fan beam filter of the Philips Aura CT scanner, as listed in the left column of Table 1, are accounted for.

The fan beam filtering has the effect of modifying the angular distribution of the air kerma in the beam. Fig. 6a and b show the two-dimensional air kerma profiles in the transversal plane of the fan beam at isocentre distance by neglecting (a) or including (b) the fan beam filtration of the single-slice Philips Aura scanner. As clearly shown in the illustrations, the fan beam filtering has the effect of turning the transversal air kerma profile from a cap shape without filtering into a wedge shape after filtering.

This circumstance has ramifications for the magnitude of the conversion factors. As becomes clear from Fig. 6, fan beam filtering has the effect of reducing the maximum doses at the same DLP more in organs and tissues located peripheral to the rotation axis than in organs near the axis. In that way, organ doses are reduced in peripherically located organs, e.g. the mammae doses (Fig. 7a) by about 20% and the kidney

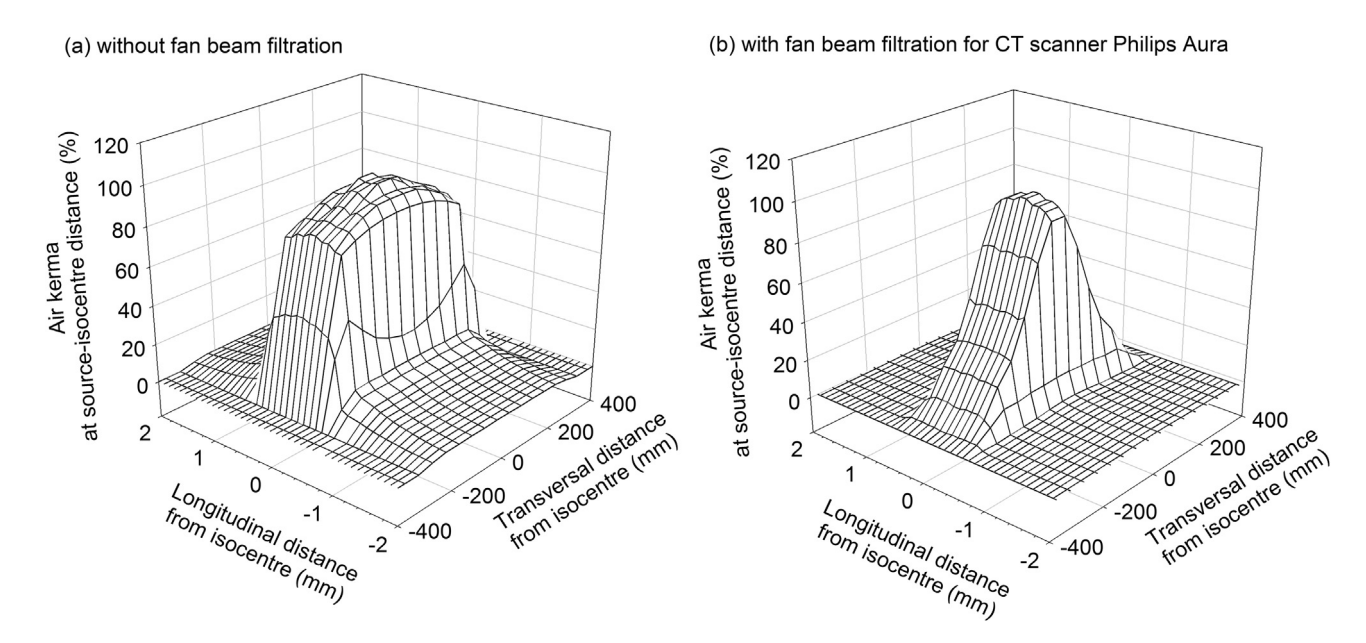


Figure 6. a, b. 2-dimensional air kerma profile in the transversal plane of a fan beam at isocentre distance, plotted for the longitudinal and the transversal direction, without (a) and with (b) fan beam filtration of the CT scanner Philips Aura.

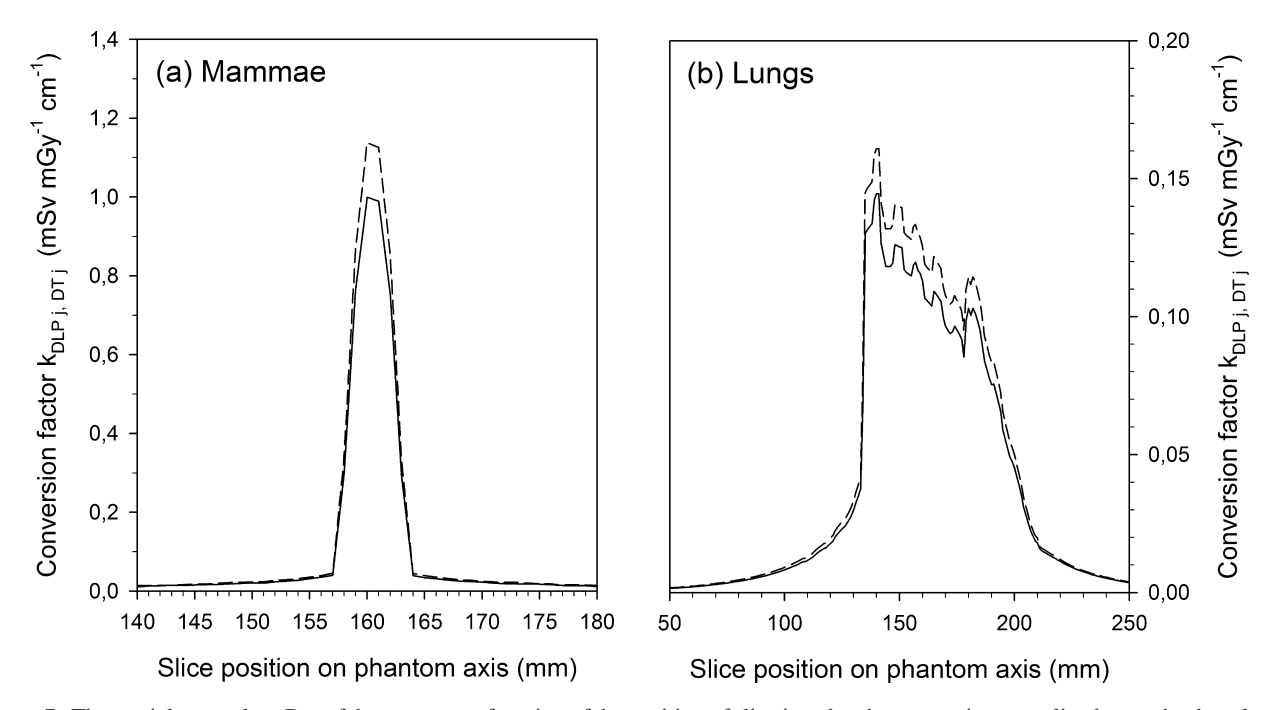


Figure 7. The partial organ dose $D_{T,j}$ of the neonate as function of the position of slice j on the phantom axis, normalized upon the dose-length product DLP_j , for slice collimation s = 1 mm and SID = 50 cm at radiation quality 120 kV + 1.5 Al + 0.07 mm Cu without (dashed line) and with fan beam filtration of the CT scanner Philips Aura (solid line).

and lung doses (Fig. 7b) by about 10%. For the thyroid which is located near the patient axis the fan beam filtering merely has the effect of reducing the radiation dose by 5%. Also for the brain, located approximately in rotation symmetry, the maximum dose reduction comes to about 5%.

3.4 Effect of patient age on the dose profiles

Due to variation of the anthropometric dimensions with patient age [46], the CT conversion factors indicate a dependence on age [47,48]; they decrease with the age of the patient, and the highest readings are found in the neonatal age group (Fig. 8). This effect, occuring with all organs and tissues, is primarily caused by the increase in the size of the organs with advancing age since the partial organ dose D_{Tj} constitutes the contribution of the 1 mm thick fan beam slice to the whole organ dose.

3.5 Example: Calculation of organ doses achieved during a HRCT examination of a six-month-old female patient

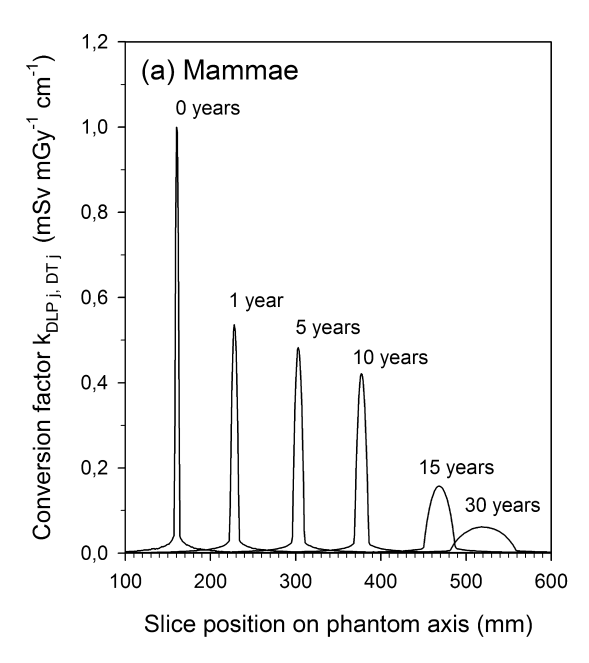
To illustrate the practical application of the method presented in eq. (12), the organ doses of the lungs, mammae, thyroid, brain and red bone marrow in a thoracic CT examination of a new-born child have been determined as an example. The CT examination was carried out on a six-months-old female patient with broncho-pulmonary dysplasia (BPD). Since BPD constitutes a generalised lung disease, the use of a

low-dose procedure of high-resolution CT (HRCT) consisting of a few single slices with large slice distances made it possible to refrain from performing a comparatively high-dose multi-slice or helical CT scan. The exposure data of the HRCT examination (high-resolution protocol 1/15) are presented in Table 3.

The 1 mm thick slices were positioned at the levels of the thoracic vertebral bodies (TVB), TVB 2, TVB 4, TVB 6 and TVB 8. Slice no. 2 was at the level of the left mammary gland. The actual position of the four slices could be determined with a precision of one half of the vertebral body height. These

Table 3
Exposure parameters of a HRCT examination of a 6 months old girl.
The HRCT examination was performed using 4 single slices with a beam aperture of 1 mm and a slice to slice distance of 15 mm (see Fig. 11).

| CT protocol | High Resolution 1/15 | | |
|--|----------------------|--|--|
| Number of single slices | 4 | | |
| Beam aperture (mm) | 1.0 | | |
| Slice to slice distance (mm) | 15 | | |
| Source-isocentre distance SID (cm) | 51.5 | | |
| Tube voltage (kV) | 130 | | |
| mAs product per single slice (mAs) | 90 | | |
| Normalized CTDI in air (mGy/mAs) | 0.41 | | |
| CTDI in air (mGy) | 36.9 | | |
| CTDI _{vol} , 16 cm PMMA (mGy) | 1.5 | | |
| CTDI _{vol} , 32 cm PMMA (mGy) | 0.72 | | |
| DLP per single slice (mGy \times cm) | 3.69 | | |



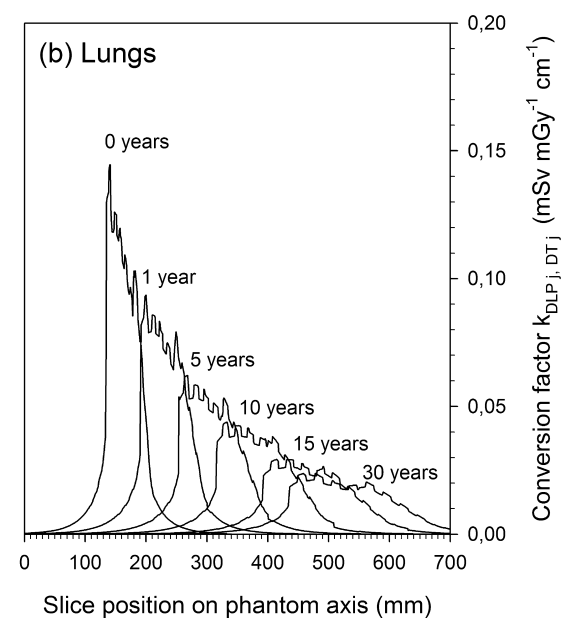


Figure 8. The partial organ dose $D_{T,j}$ for (a) mammae and (b) lungs, of a neonate, of a 1 year, 5 year, 10 year or 15 year old and for an adult patient as function of the position of slice j on the phantom axis, normalized upon the dose-length product DLP_j , for slice collimation s = 1 mm and SID = 50 cm at radiation quality 120 kV + 1.5 Al + 0.07 mm Cu under fan beam filter conditions of the CT scanner Philips Aura.

anatomic coordinates were transformed into the metrical axis coordinates of the STUK-MIRD phantoms used as the abscissas in Fig. 5. Since the body weight of the infant was 4 kg at the time of the HRCT examination, the calculation of the organ doses was performed on the basis of the conversion factors for the neonate phantom whose standard weight is 3.51 kg.

All of the organ doses D_T are composed of the *partial organ doses* $D_{T,j}$ shown in Fig. 10 as functions of slice position j. The positions of the four single slices (j=1, 2, 3, 4) are also indicated. For each 1 mm slice the same DLP of 3.69 mGy cm was assumed. Therefore, the proportion of the peak heights is the same as in Fig. 5. In this specific instance it is assumed that the mammae are included in the fan beam of single slice no. 2 while the thyroid gland or the brain only receive very low scattered contributions. The lungs are affected by all four single slices. By adding up the dose contributions by the four single slices, the organ doses listed in Table 4 are obtained.

Table 4
Organ doses achieved during the 4-slice HRCT examination of the 6 months old female patient with a slice thickness of 1 mm and a DLP per slice of 3.69 mGy cm.

| Organ T | Organ dose D _T (mSv) |
|-----------------|---------------------------------|
| Lungs | 1.4 |
| Mammae | 3.8 |
| Thyroid | 0.15 |
| Brain | 0.01 |
| Red bone marrow | 0.17 |

As illustrated by the narrow, high peak in Fig. 10, the organ dose to the mammae critically depends on the exact position of the HRCT slice. Depending on whether a small organ is centrally or only tangentially met by a CT slice, the conversion factor may differ by one order of magnitude. Due to the uncertainty entailed by visual slice positioning it is of significance for the reconstruction of a valid organ dose if the organ is showing up in the tomogram of a single slice. Fig. 9 shows that in this specific instance only the left mamma was met by an HRCT slice (slice no. 2). The organ dose given in Table 4 and Fig. 10 therefore only applies to the left mamma. Theoretically, the attempt can be made of totally avoiding slice positioning on the mammae, but positioning can only be performed with an uncertainty of about one-half of a vertebral body height.

4 Discussion

In this study the new XCT algorithm for calculating the conversion factors for the determination of applied organ doses for children of all age groups was developed in the framework of narrow-collimation single-slice high-resolution computed tomography (HRCT) examinations. The algorithm allows for application of the PCXMC algorithm originally developed for dose calculations in conventional planar radiography to the beam geometry of HRCT. Conversion factors $k_{DLP,DT,j}$ for the calculation of partial organ doses $D_{T,j}$ from the DLP $_j$ readings of single slices j according to equations (8) through (10) constitute the main result. These values will be made available elsewhere in tableworks.

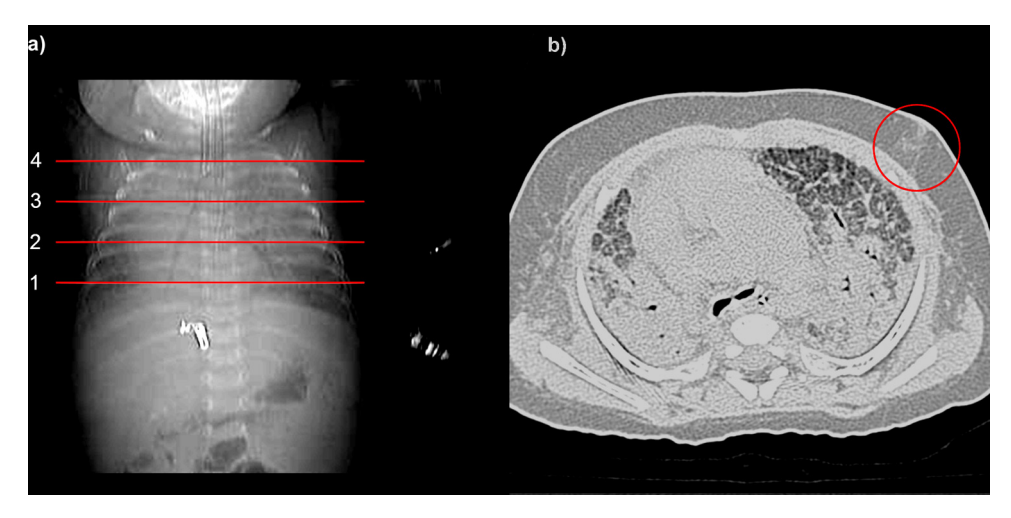


Figure 9. HRCT examination of a six months old female infant with extralobar sequestration and coiling of the feeding vessels. (a) Topogram of the chest and upper abdomen. The four slices are indicated by the numbered red lines. (b) Axial 1 mm thin slice performed in position nr. 2. The lung tissue is greatly abnormal by engorged lymphatics. The left mammary gland tissue is visible (red circle).

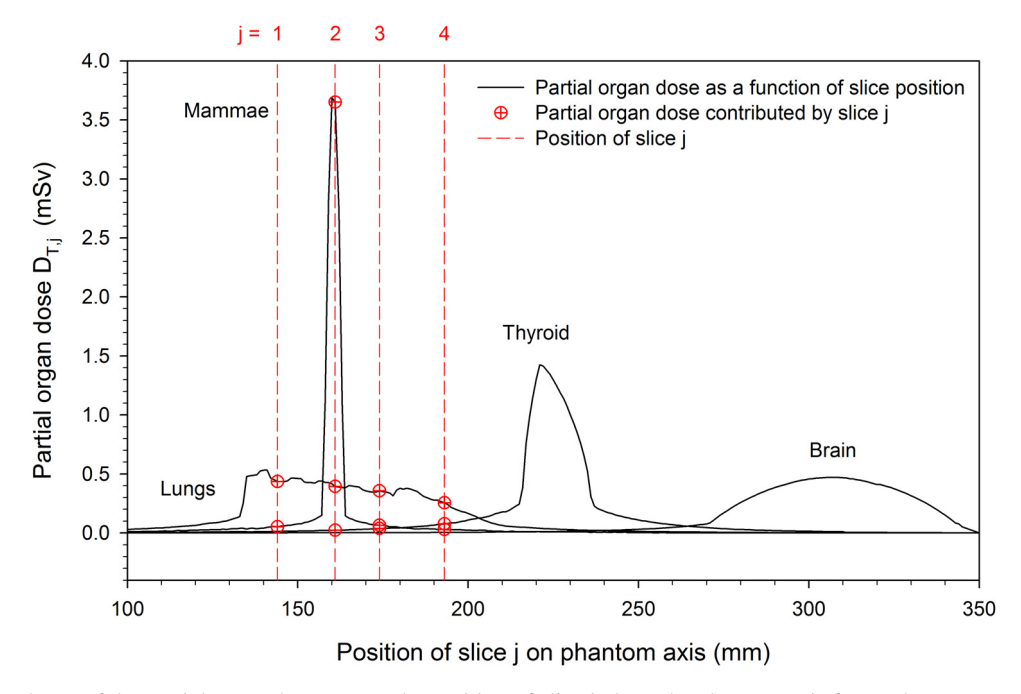


Figure 10. Dependence of the partial organ dose $D_{T,j}$ on the position of slice j along the phantom axis for T=lungs, mammae, thyroid and brain, for an HRCT examination with s=1 mm and DLPj=3.69 mGy cm. For a slice series with $DLP_j=3.69$ mGy cm for each slice, the organ doses D_T would be obtained as the sum of the partial doses $D_{T,j}$ received in this series. The red dashed lines are marking the slice positions in the 4-slice, the red circles the partial organ doses $D_{T,j}$ achieved by the single slices.

The validity of the new procedure was verified by comparison with the conversion factors given by Zankl et al. [18,19]. The conversion factors calculated for the mathematical MIRD neonate phantom, based on identical exposure conditions (Table 1), correlate well with the values given by Zankl et al. for the "Baby" voxel phantom. This also allows one to conclude that the mathematically constructed STUK-MIRD phantom of the neonate in regard to its anatomical properties

correlates well with the voxel phantom reconstructed from CT cross-section images of a genuine patient.

Whereas in the tables given by Zankl et al. [18,19] a beam aperture of 10 mm was assumed, in narrow-collimation single-slice high-resolution computed tomography a beam aperture of 1 to 1.5 mm is generally applied. Moreover, at the time of publication of the tables by Zankl et al., there was as yet no necessity of taking fan beam filtering into account.

Consequently, in the present study new conversion factors were calculated taking a beam aperture of 1 mm as a base and considering a variety of fan beam filtrations. The results are presented by way of examples based on the specific conversion factors calculated for the single-slice Philips Aura CT scanner (Figs. 7 and 8). The methodology may also be transferred to CT scanners of other manufaturers provided that the characteristics of the fan beam filtration are known.

As shown in Fig. 5, for small organs in neonates such as the mammae, the narrow-beam conversion factors (red curves) are partly higher, partly lower than the wide-beam conversion factors (black curves), since the latter are simply the mean values of the former over a width of 10 mm as shown in the introduction. All parts of Fig. 5 confirm that these mean values are in very good agreement with the values published by Zankl et al. [18,19]. Narrow beam conversion factors have the advantage to provide the precise organ doses in the case of small organs and narrow collimation. This fact should be taken into account in studies to establish the stochastic radiation risk of premature and neonatal patients. The dose readings with small-dimensioned organs and tissues are essentially determined by the position of the single slice HRCT in relation to the organ, cf. equation (12) as well as Figs. 7 and 8 and Fig. 10. Any misjudgement in localising the true beam aperture by only a few mm can by itself entail an erroneous estimate of the organ dose of the mammae by approximately one order of magnitude. Therefore in dose reconstructions, it appears as advisable to use the organ dose to the mammae in terms of a conservative estimate of radiation exposure.

Our calculations point to the chance of an effective reduction of the dose to a small organ at risk possibly achievable by deliberately arranging narrowly collimated single slices to omit this small organ. However, a small organ such as the mamma is hardly distinguishable in the topogram. Therefore, in paediatric radiological practice, complete or partial exposure of the mammae has been excluded with a high probability by adjusting the beam aperture so that the thoracic vertebral body TVB 6 was not met by the field of radiation. This technique has been applied in about 10% of all paediatric chest CT examinations.

The presented method of organ dose calculation, in addition to allowing for higher local resolution, also makes it possible to take account of a variety of fan beam filtrations according to equations (13) and (14). As could be shown in this study taking the single-slice Philips Aura CT scanner as an example, fan beam filtering with its reduction of single organ doses by up to 20% possesses a non-negligible influence on the radiation exposure of organs and tissues located peripherally to the rotation axis. This confirms the results previously obtained with an adult head phantom of 8 cm radius [49].

Unlike the geometric uncertainties in reconstructing doses in small organs, the stochastic error entailed by the Monte Carlo method is relatively small in calculations of radiation energy deposition in the organs and tissues of the mathematical MIRD phantoms. With the given number of photon histories observed, the stochastic error per fan beam due to the PCXMC algorithm was normally about 10-20% for the organs and tissue met by the primary field of radiation. Moreover, a comparison of our PCXMC dose calculations for issues of planar projection radiography with other authors (e.g. [31]) yielded a deviation of only a few per cent.

The presented conversion factors for the first time offer the opportunity of a more precise estimate of the organ doses administered to small organs in young infants and young children in paediatric HRCT, whereas for the larger organs the accuracy of previous dose evaluation codes has proven to be appropriate. In a further study, a survey will be given of the diversity of the reconstructed k_{DLPDT} organ doses that have occurred in clinical HRCT examinations of neonates and young children using different kVp and mA settings. The computation techniques developed in this study can also be used to estimate the organ doses associated with new CT scanners applied in paediatric CT examinations which are today based on multi-detector technique using wide collimations for fast volume scanning of the chest but can also be used for traditional narrow-collimation single-slice high-resolution computed tomography by combining two detector rows of 0.5 to 0.75 mm width to achieve a narrow collimation of 1.0 to 1.5 mm in a similar way as with the former single-slice scanner Philips Aura, the subject of the present study.

Acknowledgements

The authors wish to express their special gratitude to Mr. Eduard Berthold of Philips Health Care, Germany, for providing the relevant dosimetric data of the Philips Aura CT scanner operated at Dr. von Hauner's Children's Hospital.

References

- [1] Regulla D, Eder H. Patient exposure in medical X-ray imaging in Europe. Radiat Prot Dosim 2005;114:11–25.
- [2] Krille L, Zeeb H, Jahnen A, Mildenberger P, Seidenbusch M, Schneider K, Weisser G, Hammer G, Scholz P, Blettner M. Computed tomographies and cancer risk in children: a literature overview of CT practices, risk estimations and an epidemiologic cohort study proposal. Radiat Environ Biophys 2012;51:103–11.
- [3] Berrington de González A, Kim KP, Samet JM. Radiation-induced cancer risk from annual computed tomography for patients with cystic fibrosis. Am J Respir Crit Care Med 2007:176:970–3.
- [4] Brenner DJ, Elliston CD, Hall EJ, Berdon WE. Estimated Risks of Radiation-Induced Fatal Cancer from Pediatric CT. AJR 2001;176:289–96.
- [5] Brenner DJ. Estimating cancer risks from pediatric CT: going from the qualitative to the quantitative. Pediatr Radiol 2002;32:228–31.
- [6] Desmond AN, O'Regan K, Curran C, McWilliams S, Fitzgerald T, Maher MM, Shanahan F. Crohn's disease: factors associated with exposure to high levels of diagnostic radiation. Gut 2008;57:1524–9.
- [7] M'kacher R, Violot D, Aubert B, et al. Premature chromosome condensation associated with fluorescence in situ hybridisation detects cytogenetic abnormalities after a CT scan: evaluation of the low-dose effect. Radiat Prot Dosim 2003;103:35–40.

- [8] Stephan G, Schneider K, Panzer W, et al. Enhanced yield of chromosome aberrations after CT examinations in paediatric patients. Int J Radiat Biol 2007;83:281–7.
- [9] United Nations Scientific Committee on the Effects of Atomic Radiation (UNSCEAR). UNSCEAR 2013 Report, Volume II: Scientific findings on effects of radiation exposure of children, Scientific Annex B: Effects of radiation exposure of children. ISBN 978-92-1-142293-1, United Nations, New York, 2013.
- [10] Wakeford R. Childhood leukaemia following medical diagnostic exposure to ionising radiation in utero or after birth. Radiat Prot Dosim 2008:132:166–74.
- [11] Mathews JD, Forsythe Av, Brady Z, Butler MW, Goergen SC, Byrnes GB, Giles GG, Wallace AB, Anderson PR, Guiver TA, McGale P, Cain TM, Dowty JG, Bickerstaffe AC, Darby SC. Cancer risk in 680 000 people exposed to computed tomography scans in childhood or adolescence: data linkage study of 11 million Australians. BMJ 2013;346: f2360.
- [12] Pearce MS, Salotti JA, Little MP, McHugh K, Lee C, Kim KP, Howe NL, Ronckers CM, Rajaraman P, Craft AW, Parker L, Berrington de González A. Radiation exposure from CT scans in childhood and subsequent risk of leukaemia and brain tumours: a retrospective cohort study. Lancet 2012;380:499–505.
- [13] Webb WR, Müller NL, Naidich DP. Technical Aspects of High-Resolution Computed Tomography. In: Webb WR, Müller NL, Naidich DP, editors. High-resolution CT of the lung. Lippincott Williams & Wilkins; 2009. p. 1–41.
- [14] Ambrosino MM, Genieser MB, Roche KJ, Kaul A, Lawrence RM. Feasibility of high-resolution, low-dose chest CT in evaluating the pediatric chest. Pediatr Radiol 1994;24:6–10.
- [15] Copley SJ, Coren M, Nicholson AG, Rubens MB, Bush A, Hansell DM. Diagnostic Accuracy of Thin-Section CT and Chest Radiography of Pediatric Interstitial Lung Disease. AJR 2000;174:549–54.
- [16] Prosch H, Schaefer-Prokop CM, Eisenhuber E, Kienzl D, Herold CJ. CT protocols in interstitial lung diseases - A survey among members of the European Society of Thoracic Imaging and a review of the literature. Eur Radiol 2013;23:1553–63.
- [17] Deutsches Institut für Normung (DIN). Klinische Dosimetrie Teil 3: Röntgendiagnostik. DIN Norm 6809-3, 2009.
- [18] Zankl M, Panzer W, Drexler G. Tomographic Anthropomorphic Phantoms Models Part II: Organ Doses from Computed Tomography Examinations in Paediatric Radiology. GSF Forschungszentrum für Umwelt und Gesundheit, Neuherberg, Germany, GSF-Bericht 30/93; 1993.
- [19] Zankl M, Panzer W, Drexler G. The Calculation of Dose from External Photon Exposures Using Reference Human Phantoms and Monte Carlo Methods Part VI: Organ Doses from Computed Tomography Examinations. GSF Forschungszentrum für Umwelt und Gesundheit, Neuherberg, Germany, GSF-Bericht 30/91; 1991.
- [20] Jones DG, Shrimpton PC. Survey of CT Practice in the UK. Part 3: Normalised Organ Doses Calculated using Monte Carlo Techniques. In: National Radiological Protection Board. Report NRPB-R250. 1991.
- [21] Jones DG, Shrimpton PC. Normalised Organ Doses Calculated using Monte Carlo Techniques. National Radiological Protection Board, Report NRPB-SR250; 1991.
- [22] Kalender WA, Schmidt B, Zankl M, Schmidt M. A PC program for estimating organ dose and effective dose values in computed tomography. Eur Radiol 1999;9:555–62.
- [23] LeHeron JC. CTDose a computer program to enable the calculation of organ dose and dose indices for CT examinations. In: Christchurch. New Zealand: Ministry of Health, National Radiation Laboratory; 1993.
- [24] National Board of Health National Institute of Radiation Hygiene. The CT-Dose calculation program. Internet: http://freja.mta.aaa.dk/ctdose/
- [25] ImPACT. Medical Physics Department, St. George' Healthcare NHS Trust, London. Internet: http://www.impactscan.org
- [26] Stamm G, Nagel HD. CT-Expo ein neuartiges Programm zur Dosisevaluierung in der CT. Fortschr Röntgenstr 2002;174:1570–6.

- [27] Abdullah A, Sun Z, Pongnapang N, Ng KH. Comparison of computed tomography dose reporting software. Radiat Prot Dosim 2012;151:153–7.
- [28] Zankl M. Methods for assessing organ doses using computational models. Radiat Prot Dosim 1998;80:207–12.
- [29] Kramer R, Zankl M, Williams G, et al. The Calculation of Dose from External Photon Exposures Using Reference Human Phantoms and Monte Carlo Methods. Part I: The Male (Adam) and Female (Eva) Adult Mathematical Phantoms. GSF-Forschungszentrum für Umwelt und Gesundheit, Neuherberg, Germany, GSF-Bericht 1986.
- [30] Servomaa A, Rannikko S, Nikitin V, et al. A topographically and anatomically unified phantom model for organ dose determination in radiation hygiene. Finnish Centre for Radiation and Nuclear Safety, Helsinki, STUK-A87 1989.
- [31] Petoussi-Henß N, Zankl M, Fill U, et al. The GSF family of voxel phantoms. Phys Med Biol 2002;47:89–106.
- [32] Zankl M, Veit R, Williams G, et al. The construction of computer tomographic phantoms and their application in radiology and radiation protection. Radiat Environ Biophys 1988;27:153–64.
- [33] Andreo P. Monte Carlo techniques in medical radiation physics. Phys Med Biol 1991;36:861–920.
- [34] Rogers DWO. Fifty years of Monte Carlo simulations for medical physics. Phys Med Biol 2006;51:R287–301.
- [35] Nelson WR, Hirayama H, Rogers DWO. The EGS4 System, Version 4. Stanford Linear Accelerator Center Report 1985;265.
- [36] Kleinschmidt C. EGS-Ray, ein Programm zur Visualisierung von Monte-Carlo-Rechnungen in der Strahlenphysik. Z Med Phys 2001;11:119–23.
- [37] Servomaa A, Tapiovaara M. Organ dose calculation in medical X-ray examinations by the program PCXMC. Radiat Prot Dosim 1998;80:213–9.
- [38] Tapiovaara M, et al. PCXMC. A PC-based Monte Carlo program for calculating patient doses in medical x-ray examinations. Finnish Centre for Radiation and Nuclear Safety, Säteilyturvakeskus (STUK), Report STUK A-139 1997.
- [39] Cristy M. Mathematical phantoms representing children of various ages for use in estimates of internal dose. Oak Ridge Laboratory, NUREG/CR-1159, ORNL/NUREG/TM-367 1980.
- [40] International Commission on Radiological Protection: Report of the Task Group on Reference Man: Anatomical, Physiological and Metabolic Characteristics. Pergamon Press, Oxford, ICRP Publication 23; 1975.
- [41] Seidenbusch MC, Regulla D, Schneider K. Radiation Exposure of Children in Pediatric Radiology. Part 2: The PAEDOS Algorithm for Computer-Assisted Dose Reconstruction in Pediatric Radiology and Results for X-Ray Examinations of the Skull. Fortschr Röntgenstr 2008;180:522–39.
- [42] Seidenbusch MC, Regulla D, Schneider K. Radiation Exposure of Children in Pediatric Radiology. Part 3: Conversion Coefficients for Reconstruction of Organ Doses Achieved During Chest X-ray Examinations. Fortschr Röntgenstr 2008;180:1061–81.
- [43] Seidenbusch MC, Regulla D, Schneider K. Radiation Exposure of Children in Pediatric Radiology Part 6: Conversion Factors for Reconstruction of Organ Dose in Abdominal Radiography. Fortschr Röntgenstr 2009;181:945–61.
- [44] Seidenbusch MC, Regulla D, Schneider K. Radiation Exposure of Children in Pediatric Radiology. Part 7: Conversion Factors for Reconstruction of Organ Dose during Thoracoabdominal Babygrams. Fortschr Röntgenstr 2010;182:415–21.
- [45] Tapiovaara M, Siiskonen T. PCXMC 2.0. User' Guide. Finnish Centre for Radiation and Nuclear Safety, Säteilyturvakeskus (STUK), Report STUK-TR 7 2008.
- [46] Bohmann I. Ermittlung des Durchstrahlungsdurchmessers bei Säuglingen, Kindern und Jugendlichen zur Aufstellung von Belichtungswerten in der Röntgendiagnostik und Abschätzung der Organdosiswerte

- bei typischen Röntgenuntersuchungen. GSF-Forschungszentrum für Umwelt und Gesundheit Neuherberg, GSF-Bericht 16/90 1990.
- [47] Martin CJ, Farquhar B, Stockdale E, McDonald S. A study of the relationship between patient dose and size in paediatric radiology. Br J Radiol 1994;67:864–71.
- [48] Nagel HD, editor. Radiation Exposure in Computed Tomigraphy: Fundamentals, Influencing Parameters, Dose Assessment, Optimisation,
- Scanner Data, Terminology. CTB Publications, Hamburg, Germany, published by: European Coordination Committee of the Radiological and Electromedical Industries. Frankfurt, Germany: c/o ZVEI, Fachverband Electromedizinische Technik; 2002. p. 85.
- [49] Caon M, Bibbo G, Pattison J. A comparison of radiation dose measured in CT dosimetry phantoms with calculations using EGS4 and voxelbased computational models. Phys Med Biol 1997;42:219–29.

Available online at www.sciencedirect.com

ScienceDirect